ELSEVIER

Mathematics and Computers in Simulation 55 (2001) 59–66

MATHEMATICS AND COMPUTERS IN SIMULATION

www.elsevier.nl/locate/matcom

A floating random-walk algorithm for extracting electrical capacitance

Ralph B. Iverson [a], Yannick L. Le Coz [b,*]

[a] *Random Logic Corporation, 14 Gussie Terrace, Somerville, MA 02143-2249, USA*
[b] *Center for Integrated Electronics, Rensselaer Polytechnic Institute, Troy, NY, 12180-3590, USA*

Abstract

In 1991, we developed a floating random-walk algorithm to extract electrical capacitance in 2D structures. Since then, our work has evolved into a powerful commercial 3D CAD tool, *QuickCap*™, capable of finding capacitance in integrated circuits (ICs) represented by multi-gigabyte databases. The algorithm has proven to be exceptionally powerful and is now finding acceptance in an application area traditionally dominated by deterministic algorithms. We present the theory underlying the floating random-walk algorithm: a formulation of capacitance as an integral of infinite dimensionality evaluated by Monte Carlo integration. A single Monte Carlo sample of the integral corresponds to a floating random-walk. We also discuss performance characteristics of *QuickCap* and we summarize our contributions in other application areas.

Keywords: Algorithm; Capacitance; Integrated circuits; *QuickCap*

1. Introduction

Until the 1990s, the electrical speed of integrated circuits (ICs) was limited by the intrinsic properties of transistors. As devices have shrunk and as chip size has increased, however, interconnect capacitance has risen in importance. This electrical parasitic is now a dominant factor in high-speed chip design [1–4].

In many cases, 1D or 2D capacitance analysis is simply not accurate enough to meet the standards of industry. On the other hand, deterministic 3D methods are unable to analyze critical interconnects in reasonable time because of geometric complexity. In 1991, we developed a 2D floating random-walk algorithm to extract capacitance [5,6], the algorithm evolved into a 3D commercial product *QuickCap*™. Since then, this approach has been compared many times with experiment and found to agree quite well [7–11].

Other publications on the floating random-walk method use circles, spheres, cubes and other shapes [12–14]. The work we published in 1991 represents the first application of square and cube-based floating random-walk methods to find capacitance.

* Corresponding author.

0378-4754/01/$20.00
PII: S0378-4754(00)00246-9

We present here the theory underlying the floating random-walk approach, along with a discussion of the performance characteristics of *QuickCap*. We also summarize our other research relating to floating random-walks.

2. Capacitance equations

A capacitance matrix $\boldsymbol{C}$ specifies the linear relationship between the voltage vector $\boldsymbol{V}$ consisting of scalar voltages $v_i, v_j, \ldots$, at electrodes $i, j, \ldots$, and the vector $\boldsymbol{Q}$ consisting of scalar charges $q_i, q_j, \ldots$, on electrodes $i, j, \ldots$:

$$\boldsymbol{Q} = \boldsymbol{C}\boldsymbol{V}. \tag{1}$$

The capacitance matrix has elements:

$$c_{ij} = \frac{\partial q_i}{\partial v_j}. \tag{2}$$

Charge on an electrode is related to the flux of the electric field $\boldsymbol{E}(\boldsymbol{r})$ through an arbitrary closed surface S separating the electrode from all others. We have, therefore,

$$q_{\mathrm{i}} = \oint_S \hat{\boldsymbol{n}}\, \mathrm{d}S \cdot \epsilon \boldsymbol{E}, \tag{3}$$

where $\hat{\boldsymbol{n}}$ is the outward unit vector normal to S. The dielectric permittivity ϵ is a spatially constant material parameter (space-dependent ϵ is outside the scope of this paper).

Electric field is defined as the gradient of the electrostatic potential distribution:

$$\boldsymbol{E} = -\nabla_{\boldsymbol{r}}\phi. \tag{4}$$

The potential $\phi(\boldsymbol{r})$ in charge-free homogeneous materials satisfies Laplace's equation with Dirichlet boundary conditions at all electrode surfaces, $\phi = v_i$ on electrode i, $\phi = v_j$ on electrode j and so forth. Consequently,

$$\nabla^2_{\boldsymbol{r}}\phi = 0. \tag{5}$$

3. Capacitance as an infinitely nested integral

In this section, we formulate the equations for a column of the capacitance matrix $\boldsymbol{C}$ as an exact vector integral equation.

Equations for $\boldsymbol{E}$ and ϕ at any point $\boldsymbol{r}'$ can be written as integrals over the surface of an enclosing materially homogeneous volume — an electrode-free volume where $\boldsymbol{r}'$ is in its interior:

$$\phi(\boldsymbol{r}') = \oint_S \mathrm{d}S\, G_\phi(\boldsymbol{r}|\boldsymbol{r}')\phi(\boldsymbol{r}), \tag{6}$$

$$\boldsymbol{E}(\boldsymbol{r}') = \oint_S \mathrm{d}S\, \boldsymbol{G}_{\boldsymbol{E}}(\boldsymbol{r}|\boldsymbol{r}')\phi(\boldsymbol{r}). \tag{7}$$

Green's functions $G_\phi(\boldsymbol{r}|\boldsymbol{r}')$ and $\boldsymbol{G_E}(\boldsymbol{r}|\boldsymbol{r}')$ determine the voltage and electric field at a point $\boldsymbol{r}'$ inside the volume when the voltage on the surface of the volume is a 2D surface impulse function at point $\boldsymbol{r}$.

The Green's functions allow us to construct an integral equation for $\boldsymbol{C}_i$, the column of $\boldsymbol{C}$ associated with electrode i. In the following equations, this integral is broken up into individual surface integrals. Each term in curly braces represents an integral. The last line is recursive:

$$\boldsymbol{C}_i = \{\nabla_{\boldsymbol{V}} q_i\}, \tag{8}$$

$$\nabla_{\boldsymbol{V}} q_i = \oint_{S_0} \mathrm{d}S_0 \epsilon \{\hat{\boldsymbol{n}}_0 \cdot \nabla_{\boldsymbol{V}} \boldsymbol{E}(\boldsymbol{r}_0)\},$$

$$\hat{\boldsymbol{n}}_0 \cdot \nabla_{\boldsymbol{V}} \boldsymbol{E}(\boldsymbol{r}_0) = \oint_{S_1} \mathrm{d}S_1 \, [\hat{\boldsymbol{n}}_0 \cdot \boldsymbol{G_E}(\boldsymbol{r}_1|\boldsymbol{r}_0)]\{\nabla_{\boldsymbol{V}} \phi(\boldsymbol{r}_1)\},$$

$$\nabla_{\boldsymbol{V}} \phi(\boldsymbol{r}_k) = \oint_{S_{k+1}} \mathrm{d}S_{k+1} \, G_\phi(\boldsymbol{r}_{k+1}|\boldsymbol{r}_k \{\nabla_{\boldsymbol{V}} \phi(\boldsymbol{r}_{k+1})\}, \quad k = 1, 2, 3, \ldots,$$

where we define $\nabla_{\boldsymbol{V}} = [\partial/\partial v_i, \partial/\partial v_j, \ldots,]^T$.

The integral for $\nabla_{\boldsymbol{V}} q_i$ is over a surface S_0 enclosing electrode i. Each subsequent integral is over surface S_{k+1} of a homogeneous volume containing $\boldsymbol{r}_k$. By selecting homogeneous volumes with surfaces that are in part coincident with surfaces of one or more electrodes, each integral for electric field and voltage will include a term that is not, itself, another integral. When $\boldsymbol{r}_k$ is on the surface of electrode j, the jth element of $\nabla_{\boldsymbol{V}} \phi(\boldsymbol{r}_k)$ is unity and the other elements are zero.

4. *Quickcap* implementation

QuickCap evaluates the integrals in Eq. (8) by Monte Carlo integration using Green's functions for 'maximal cubes'. A maximal cube is the largest homogeneous cube centered at $\boldsymbol{r}_0$, limited in size by the nearest electrode. Establishing the maximal cube associated with a point generally involves simple operations using the coordinates of the electrode surfaces.

For a cube extending from (0, 0, 0) to (L, L, L), the Green's function G_ϕ for potential inside the cube with a voltage $\delta(x' - x)\delta(y' - y)$ at the cube top $z = L$ is

$$G_\phi(x, y, L|x', y', z') = \frac{4}{L^2} \sum_{n_{x=1}}^{\infty} \sum_{n_{y=1}}^{\infty} \sin\left(\frac{\pi n_x}{L} x'\right) \sin\left(\frac{\pi n_y}{L} y'\right) \sinh\left(\frac{\pi n_z}{L} z'\right) \times \frac{\sin\{(\pi n_x/L)x\} \sin\{(\pi n_y/L)y\}}{\sinh(\pi n_z)}, \tag{9}$$

where $n_z = (n_x^2 + n_y^2)^{1/2}$. Similar functions can be written for the other cube faces (see [6] for 2D analysis).

From Eq. (4), the Green's function $\boldsymbol{G_E}$ for the electric field inside the cube is:

$$\boldsymbol{G_E}(x, y, L|x', y', z') = \frac{4}{L^2}\sum_{n_x=1}^{\infty}\sum_{n_y=1}^{\infty}\begin{bmatrix} \frac{-\pi n_x}{L}\cos\left(\frac{\pi n_x}{L}x'\right)\sin\left(\frac{\pi n_y}{L}y'\right)\sinh\left(\frac{\pi n_z}{L}z'\right) \\ \frac{-\pi n_y}{L}\sin\left(\frac{-\pi n_x}{L}x'\right)\cos\left(\frac{\pi n_y}{L}y'\right)\sinh\left(\frac{\pi n_z}{L}z'\right) \\ \frac{-\pi n_z}{L}\sin\left(\frac{\pi n_x}{L}x'\right)\sin\left(\frac{\pi n_y}{L}y'\right)\cosh\left(\frac{\pi n_z}{L}z'\right) \end{bmatrix} \times \frac{\sin\{(\pi n_x/L)x\}\sin\{(\pi n_y/L)y\}}{\sinh(\pi n_z)}. \tag{10}$$

QuickCap uses Green's functions $\bar{G}_\phi$ and $\bar{\boldsymbol{G}}_{\boldsymbol{E}}$ for cubes centered about $\boldsymbol{r}'$. In the following forms, the right side of each equation can be evaluated as a function of normalized position on the top of the cube (x/L, y/L) and is independent of cube size:

$$L^2\bar{G}_\phi(x, y, L) = 2\sum_{n_x=1}^{\infty}\sum_{n_y=1}^{\infty}\frac{\sin(\pi n_x/2)\sin(\pi n_y/2)}{\cosh(\pi n_z/2)} \times \sin\left(\pi n_x\frac{x}{L}\right)\sin\left(\pi n_y\frac{y}{L}\right), \tag{11}$$

$$-L^3\bar{\boldsymbol{G}}_{\boldsymbol{E}}(x, y, L) = 2\pi\sum_{n_x=1}^{\infty}\sum_{n_y=1}^{\infty}\begin{bmatrix} \frac{n_x\cos(\pi n_x/2)\sin(\pi n_y/2)}{\cosh(\pi n_z/2)} \\ \frac{n_y\sin(\pi n_x/2)\cos(\pi n_y/2)}{\cosh(\pi n_z/2)} \\ \frac{n_z\sin(\pi n_x/2)\sin(\pi n_y/2)}{\sinh(\pi n_z/2)} \end{bmatrix} \times \sin\left(\pi n_x\frac{x}{L}\right)\sin\left(\pi n_y\frac{y}{L}\right). \tag{12}$$

These Green's functions are plotted in Figs. 1–3 for $L = 1$. Fig. 1 shows the centered voltage Green's function $\bar{G}_\phi$. Fig. 2 shows the centered Green's function for z-component of electric field $\bar{G}_{\boldsymbol{E}z}$ The strongest mode of $\bar{G}_\phi$ and $\bar{G}_{\boldsymbol{E}z}$ is $(n_x, n_y) = (1, 1)$. Fig. 3 shows the centered Green's function for y-component of electric field $\bar{G}_{\boldsymbol{E}y}$. The strongest mode of $\bar{G}_{\boldsymbol{E}y}$ is $(n_x, n_y) = (1, 2)$.

Each Monte Carlo sample for the capacitance determined by Eq. (8) requires a series of following points.

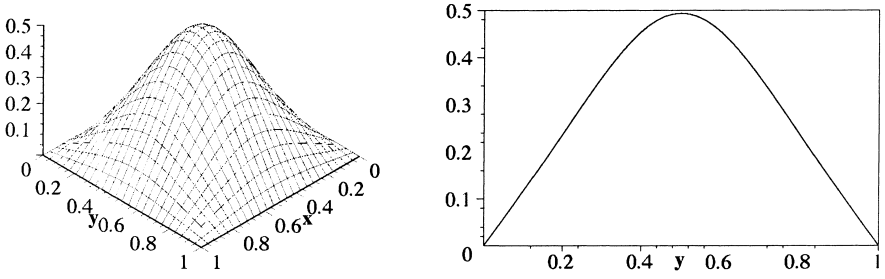

Fig. 1. $\bar{G}_\phi$ for $L = 1$: at $z = L$ (left) and at $x = L/2$, $z = L$ (right).

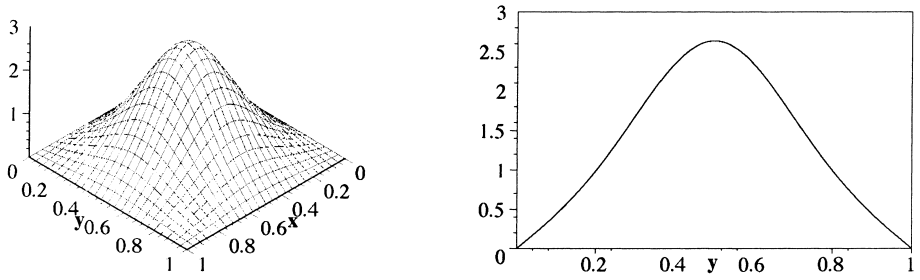

Fig. 2. $-\bar{\boldsymbol{G}}_{\boldsymbol{E}z}$ for $L = 1$: at $z = L$ (left) and at $x = L/2$, $z = L$ (right).

- The first point $\boldsymbol{r}_0$ is selected with uniform probability on a surface enclosing electrode i, $\hat{\boldsymbol{n}}_0 \cdot \nabla_{\boldsymbol{V}} \boldsymbol{E}(\boldsymbol{r}_0)$ needs to be evaluated and then scaled by ϵA_0 where A_0 is the area of the surface enclosing electrode i.
- $\hat{\boldsymbol{n}}_0 \cdot \nabla_{\boldsymbol{V}} \boldsymbol{E}(\boldsymbol{r}_0)$ is evaluated by selecting a point $\boldsymbol{r}_1$ on the surface of the maximal cube enclosing $\boldsymbol{r}_0$ according to a probability density function $P_{\boldsymbol{E}}(\boldsymbol{r}_1|\boldsymbol{r}_0)$, evaluating $\nabla_{\boldsymbol{V}}\phi(\boldsymbol{r}_1)$ and scaling by $[\boldsymbol{G}_{\boldsymbol{E}}(\boldsymbol{r}_1|\boldsymbol{r}_0) \cdot \hat{\boldsymbol{n}}_0]/P_{\boldsymbol{E}}(\boldsymbol{r}_1|\boldsymbol{r}_0)$. Ideally, $P_{\boldsymbol{E}}$ is the same shape as $|\boldsymbol{G}_{\boldsymbol{E}}(\boldsymbol{r}_1|\boldsymbol{r}_0) \cdot \hat{\boldsymbol{n}}|$, in which case the scale is $\pm K_{\boldsymbol{E}}/L_1$ where $K_{\boldsymbol{E}}$ is a constant, L_1 the cube size and the sign depends on the point selected on the cube surface.
- Until $\boldsymbol{r}_k$ is on the surface of an electrode, $\nabla_{\boldsymbol{V}}\phi(\boldsymbol{r}_k)$ is found by selecting a point $\boldsymbol{r}_{k+1}$ on the surface of a maximal cube enclosing $\boldsymbol{r}_k$ according to a probability density function $P_\phi(\boldsymbol{r}_{k+1}|\boldsymbol{r}_k)$, evaluating $\nabla_{\boldsymbol{V}}\phi(\boldsymbol{r}_{k+1})$ and scaling by $G_\phi(\boldsymbol{r}_{k+1}|\boldsymbol{r}_k)/P_\phi(\boldsymbol{r}_{k+1}|\boldsymbol{r}_k)$. Ideally, $P_\phi(\boldsymbol{r}_{k+1}|\boldsymbol{r}_k)$ is exactly $G_\phi(\boldsymbol{r}_{k+1}|\boldsymbol{r}_k)$, in which case no scaling need be applied.
- When $\boldsymbol{r}_k$ is on an electrode surface, $\nabla_{\boldsymbol{V}}\boldsymbol{V}(\boldsymbol{r}_k)$ is an incidence vector, with a single nonzero element equal to unity corresponding to the electrode at $\boldsymbol{r}_k$.

The series of points for a Monte Carlo sample defines a floating random-walk. Each maximal cube is limited in size by the nearest electrode, resulting in a variable hop size ($k = 0, 1, 2, \ldots,$). A conventional floating random-walk method [12] implements maximal spheres (or circles) that do not conform well to the mostly rectilinear IC-interconnect geometry.

For ideal sampling density functions, each Monte Carlo sample is bounded in value by $\pm\epsilon A_0 K_{\boldsymbol{E}}/L_{\min}$ where $L_{\min}$ is the size of the smallest maximal cube on the surface enclosing electrode i. Convergence is, therefore, guaranteed for ideal sampling density functions.

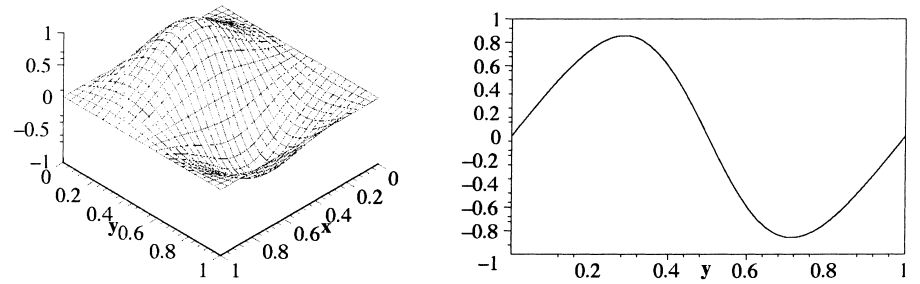

Fig. 3. $-\bar{\boldsymbol{G}}_{\boldsymbol{E}y}$ for $L = 1$: at $z = L$ (left) and at $x = L/2$, $z = L$ (right).

5. Performance characteristics

Performance characteristics summarized in this section include bias error, speed versus complexity and memory versus accuracy. Standard deterministic methods, to list a few, employ a volumetric or areal surface-electrode mesh, or use a moment-integration, Fourier decomposition, or spectral method [16–20]. These methods introduce numerical discretization error which can be reduced only by increasing either the mesh density, the number of moments or the number of Fourier modes. This increases, as well, both the run time and memory usage. Extracting capacitance with any of these methods to reasonable accuracy, say ±1% for large, realistic IC-interconnect structures requires significantly more run time and more memory than *QuickCap*.

5.1. Bias

Bias is the error of a statistical sampling method in the limit of infinite samples. *QuickCap*'s bias includes: (i) any inaccuracies in the random-number generator, (ii) approximations for the Green's functions and (iii) spatial discretization error (the *QuickCap* kernel uses integer coordinates with a resolution 1 Å). Table 1 lists *QuickCap* bias derived from exact, analytical solution of some simple capacitance problems. We conclude with a high level of confidence that the bias is less than ±0.03%. Because complex problems do not introduce any differences to the algorithm, the bias on more complex problems is probably about the same, negligible, in fact, compared to typical 5–10% effects due to IC-process variation. Deterministic methods generally produce discretization error and require boundary-condition approximations that lead to much larger errors, except for simple problems that permit fine discretization and distant boundaries.

5.2. Speed versus complexity

A study comparing *QuickCap* to two deterministic methods was published [21]. *QuickCap* convergence time was found to vary weakly with 'complexity', that is, with the length of the extracted electrode and with the number of other electrodes involved. The extraction time of a 2 μm electrode coupled to one other electrode was practically identical, for the same accuracy, to that of a 2 mm electrode coupled to 1000 other electrodes. Deterministic methods, in contrast, require at least 1000 times as much run time on the more complex problem. For problems with more than two electrodes, at a statistical error of ±1%, *QuickCap* was faster than the deterministic methods we studied operating at discretization errors of ±1%.

Typical *QuickCap* execution times are on the order of a minute or so for ±1% accuracy. Naturally, this varies with the speed of the computer. As should be expected, the statistical error decreases as the square root of the run time.

Table 1
QuickCap bias for simple problems with exact, analytical solutions [15]

Problem description	Bias (%)
1D: parallel plates	-0.002 ± 0.001
2D: parallel circular wires	-0.018 ± 0.004
3D: sphere in free space	$+0.002 \pm 0.004$

5.3. Memory versus accuracy

Unlike deterministic methods, *QuickCap* memory requirements are independent of the level of accuracy. Compared with deterministic methods [21], *QuickCap* memory requirements were found to be less than those of deterministic methods by three to seven orders of magnitude. All methods were evaluated at the same level of error.

6. Other application areas

Our other work with floating random-walk capacitance extraction involves dielectric anisotropy [9–11] and effects of using Monte Carlo capacitance results in modeling distributed and crosstalk capacitance [22,23]. We have applied the floating random-walk approach to thermal, magnetic inductance and full-wave electromagnetic problems.

The floating random-walk method was used to find detailed thermal fields in IC-multichip-module interconnects [24]. For this case, steady-state temperature $T(\boldsymbol{r})$ obeys the Laplace equation:

$$\nabla_{\boldsymbol{r}} \cdot (\kappa \nabla_{\boldsymbol{r}} T) = 0, \tag{13}$$

with thermal conductivity $\kappa(\boldsymbol{r})$.

Currently, we are developing a multiscale local–global thermal analysis procedure to model IC-device, chip and packaging structures. [1] We solve here a more general Poisson equation:

$$\nabla_{\boldsymbol{r}} \cdot (\kappa \nabla_{\boldsymbol{r}} T) = -g. \tag{14}$$

The source term $g(\boldsymbol{r})$ represents heat generated in transistors and interconnects. Our multiscale approach employs a changing random-walk environment, during the walk itself — from a detailed local geometry to a simplified, global geometry where the chip is replaced by a thermal-equivalent model.

We have also applied the floating random-walk method to the electrical inductance problem [25]. This requires calculation of the static (frequency-independent) magnetic vector potential $\boldsymbol{A}(\boldsymbol{r})$. It has the following Poisson-equation form:

$$\nabla_{\boldsymbol{r}}^2 \boldsymbol{A} = -\mu_0 \boldsymbol{J}. \tag{15}$$

$\boldsymbol{J}(\boldsymbol{r})$ is electric current density in conductors, μ_0 a constant free-space magnetic permeability. $\boldsymbol{A}$ is subject to the boundary condition that it vanishes for large $|\boldsymbol{r}|$.

Research into full-wave electromagnetic solution by means of floating random-walks is underway [26]. We use Maxwell's equations without making approximations normally introduced when applying these equations to electric-circuit analysis. State-of-the-art integrated circuits are now fast enough that discrepancies between classical circuit analysis and observed behavior can be attributed in part to these approximations. The associated vector-potential obeys a Helmholtz equation:

$$\nabla_{\boldsymbol{r}}^2 \boldsymbol{A} - \gamma^2 \boldsymbol{A} = -\mu_0 \boldsymbol{J}. \tag{16}$$

The complex-valued propagation parameter $\gamma(\boldsymbol{r})$ is a function of material type. In general, both $\boldsymbol{J}$ and γ, and therefore $\boldsymbol{A}$, depend on excitation frequency ω.

[1] This work is currently supported by the Microelectronics Advanced Research Corporation, Contract No. 98-IT-674; the Defence Advanced Research Projects Agency, Grant No. MDA 972-99-1-0002 and New York State.

7. Conclusion

QuickCap uses a powerful method, a cube-based floating random-walk, to calculate electrical capacitance. We have presented the basic theory. We have summarized *QuickCap*'s performance characteristics. Other application areas have been reviewed.

Acknowledgements

The work of YLL is supported in part by the SRC Center for Advanced Interconnect Science and Technology, Rensselaer, Contract No. 448-048.

References

[1] J.D. Meindl, Solid-St. Tech. 30 (1987) 85.
[2] M.R. Scheinfein, et al., IEEE Trans. Comp., Hybrids, Manuf. Tech. 10 (1987) 303.
[3] D.C. Edelstein, et al., in: Proceedings of the 10th International VLSI Multilevel Interconnect Conference, Santa Clara, CA, 1993, p. 511.
[4] J.D. Meindl, IEEE Circuits and Devices 12 (1996) 19.
[5] Y.L. Le Coz, R.B. Iverson, in: Proceedings of the Eighth International VLSI Multilevel Interconnect Conference, Santa Clara, CA, 1991, p. 364.
[6] Y.L. Le Coz, R.B. Iverson, Solid-St. Electron. 35 (1992) 1005.
[7] Y.L. Le Coz, R.B. Iverson, et al., in: Proceedings of the 11th International VLSI Multilevel Interconnect Conference, Santa Clara, CA, 1994, p. 342.
[8] Y.L. Le Coz, H.J. Greub, A. Garg, J.F. McDonald, R.B. Iverson, in: Proceedings of the 13th International VLSI Multilevel Interconnect Conference, Santa Clara, CA, 1996, p. 230.
[9] Y.L. Le Coz, H.J. Greub, A. Garg, P.M. Campbell, S.A. Steidl, J.F. McDonald, R.B. Iverson, in: Proceedings of the 14th International VLSI Multilevel Interconnect Conference, Santa Clara, CA, 1997, p. 201.
[10] A. Garg, Y.L. Le Coz, J.F. McDonald, R.B. Iverson, in: Proceedings of the IEEE International Interconnect Technical Conference, San Francisco, CA, 1998, p. 241.
[11] A. Garg, Y.L. Le Coz, R.B. Iverson, et al., IEEE Trans. CAD ICs Syst. 18 (1999) 212.
[12] G.M. Brown, in: E.F. Beckenbach (Ed.), Modern Mathematics for the Engineers, McGraw-Hill, New York, 1956.
[13] A. Haji-Sheikh, E.M. Sparrow, Trans. ASME C-89, Vol. 121, 1967, see in particular, the section 'Author's Closure' and references therein.
[14] K.K. Sabelfeld, Monte Carlo Methods in Boundary Value Problems, Springer, New York, 1991, see references therein.
[15] W.L. Loh, LSI Logic, Milpitas, CA, 1999.
[16] A.E. Ruehli, P.A. Brennan, IEEE Trans. Microwave Theory Tech. 21 (1973) 76.
[17] P.E. Cottrell, E.M. Buturla, IBM J. Res. Develop. 29 (1985) 277.
[18] F.S. Lai, Solid-St. Electron. 32 (1989) 141.
[19] A.H. Zemanian, IEEE Trans. Electron Dev. 35 (1988) 985.
[20] K. Nabors, S. Kim, J. White, IEEE Trans. Microwave Theory Tech. 7 (1992) 1496.
[21] Y.L. Le Coz, H.J. Greub, R.B. Iverson, Solid-St. Electron. 42 (1998) 58.
[22] R.B. Iverson, Y.L. Le Coz, in: Proceedings of the 1997 International Conference on Simulation of Semiconductors Processes and Development, Cambridge, MA, 1997, p. 117.
[23] R.B. Iverson, Y.L. Le Coz, in: Proceedings of the IEEE Modeling and Simulation of Microsystems, Semiconductors, Sensors and Actuators, Santa Clara, CA, 1998, p. 117.
[24] Y.L. Le Coz, R.B. Iverson, et al., Numerical Heat Transfer, Part B: Fundamentals 26 (1994) 353.
[25] Y.L. Le Coz, R.B. Iverson, Q.T. Vu, in: Proceedings of the Ninth International VLSI Multilevel Interconnect Conference, Santa Clara, CA, 1992, p. 456.
[26] J.W. Perry, Y.L. Le Coz, R.B. Iverson, in: Proceedings of the 15th International VLSI Multilevel Interconnect Conference, Santa Clara, CA, 1998, p. 312.